Insights into the Subsurface Transport of As(V) and Se(VI) in Produced Water from Hydraulic Fracturing Using Soil Samples from Qingshankou Formation, Songliao Basin, China

Season S. Chen[1], Yuqing Sun[1,2], Daniel C.W. Tsang[1,*], Nigel J.D. Graham[3], Yong Sik Ok[4], Yujie Feng[2,*], Xiang-dong Li[1]

[1] Department of Civil and Environmental Engineering, The Hong Kong Polytechnic University, Hung Hom, Kowloon, Hong Kong, China.

[2] State Key Laboratory of Urban Water Resource and Environment, Harbin Institute of Technology, Harbin 150090, China.

[3] Environmental and Water Resources Engineering, Department of Civil and Environmental Engineering, Imperial College London, South Kensington, London SW7 2AZ, UK.

[4] Korea Biochar Research Center & School of Natural Resources and Environmental Science, Kangwon National University, Chuncheon 24341, Korea.

* *Corresponding author (email: dan.tsang@polyu.edu.hk, phone: 852-2766-6072, fax: 852-2334-6389).*

**Co-corresponding author (email: yujief@hit.edu.cn, phone: 86-451-86283068, fax: 86-451-87162150).*

Abstract

Produced water is a type of wastewater generated from hydraulic fracturing, which may pose a risk to the environment and humans due to its high ionic strength and the presence of elevated concentrations of metals/metalloids that exceed maximum contamination levels. The mobilization of As(V) and Se(VI) in produced water and selected soils from Qingshankou Formation in the Songliao Basin in China were investigated using column experiments and synthetic produced water whose quality was representative of waters arising at different times after well creation. Temporal effects of produced water on metal/metalloid transport and sorption/desorption were investigated by using HYDRUS-1D transport modelling. Rapid breakthrough and long tailings of As(V) and Se(VI) transport were observed in Day 1 and Day 14 solutions, but were reduced in Day 90 solution probably due to the elevated ionic strength. The influence of produced water on the hydrogeological conditions (i.e., change between equilibrium and non-equilibrium transport) was evidenced by the change of tracer breakthrough curves before and after the leaching of produced water. This possibly resulted from the sorption of polyacrylamide (PAM ($-CH_2CHCONH_2-)_n$) onto soil surfaces, through its use as a friction reducer in fracturing solutions. The sorption was found to be reversible in this study. Minimal amounts of sorbed As(V) were desorbed whereas the majority of sorbed Se(VI) was readily leached out, to an extent which varied with the composition of the produced water. These results showed that the mobilization of As(V) and Se(VI) in soil largely depended on the solution pH and ionic strength. Understanding the differences in metal/metalloid transport in produced water is important for proper risk management.

Keywords: produced water; hydraulic fracturing; arsenic; selenium; non-equilibrium transport; solution chemistry.

Introduction

Hydraulic fracturing (fracking) has significantly advanced the oil and gas extraction from low-permeability shale formations (Kargbo et al., 2010; King, 2012; Vidic et al., 2013). In 2011, the production of natural gas in the US was 23 trillion cubic feet, accounting for 95% of domestic consumption (US EIA, 2013). China has one of the largest shale reservoirs in the world (Tollefson, 2013) and the Government plans to produce 300 billion cubic metres of shale gas by 2020 (China's State Council, 2015). However, the possible adverse environmental impact and human health implications of hydraulic fracturing have aroused intense public concern and research interest on aspects including water and soil contamination (Warner et al., 2013; Vengosh et al., 2014), occurrence of radioactive material (Kondash et al., 2013; Nelson et al., 2014), and air pollution (Moore et al., 2014; Swarthout et al., 2015).

A large proportion of the hydraulic fracturing fluid returns to the surface in the first two weeks, which is the produced water generated right after hydraulic fracturing (also referred to as flowback water). Produced water is also generated during the production phase of a well, which can last for years (US EIA, 2013; Vidic et al., 2013; US EPA, 2016). Produced water contains extremely high levels of total dissolved solids (TDS) (up to 350 g L^{-1}), metal/metalloid ions, and brine salts of Ca, Ba, and Cl (Barbot et al., 2013; Ferrar et al., 2013; Jackson et al., 2013). Organic ingredients in the hydraulic fracturing fluid such as gelling agents, friction reducers, and surfactants are also recovered with produced water (Hayes, 2009; Gregory et al., 2011; Ziemkiewicz and He, 2015). The presence of biocide (e.g., glutaraldehyde) would impede the biodegradation and microbial-mediated transformation of surfactants and trace elements (McLaughlin et al., 2016).

Among the elements identified in the produced water, trace elements such as As and Se may be present at a concentration depending on the geochemical characteristics of the formation. For example, black shales in Britain and Ireland lead to excessive amounts of As and Se in groundwater after interaction with produced water (Parnell et al., 2016). It has been reported that As and Se are constituents of gas containing rock beds (Haluszczak et al., 2013), and within the Qingshankou Formation in the Songliao Basin, China, the Cretaceous black shale may possibly have Se enrichment (Zou et al., 2010) and overlap with an elevated-As region (Rodriguez-Lado et al., 2013). These elements are particularly important because the toxicity imposed by As and Se may present environmental concerns and health risks, especially when there are inadvertent spills of produced water.

The majority of inadvertent fluid spills have been reported outside the well pad (i.e., area cleared for drilling rigs), in which spills of produced water usually occur during transport and filling/clearing of the impoundments (Lauer et al., 2016). It is estimated in a sudden spill scenario that an area of 0.1 acre (404.7 m^2) could be affected by 1000 gallon (3785.4 L) of produced water (Gradient, 2012), which could cause a significant impact on soil and groundwater contamination before natural attenuation. The content of dissolved oxygen in produced water was found to increase during its storage in an impoundment, and this resulted in positive redox potentials (oxidizing) (Milligan and Reddy, 2007). The spillage of produced water is likely to be under an oxidizing environment where As can be mobilized by oxidation and dissolution of As-bearing sulphide minerals and iron oxides (Kim, et al., 2014; Phan et al., 2015). Thus, As(V) would be the predominant form of As from the produced water in the impoundment.

87 The mobility of Se is also controlled by its chemical speciation. In aerated alkaline soils, selenate
88 and selenite are the predominating species of inorganic Se, which are highly soluble. While
89 Se(IV) is strongly adsorbed by soils, Se(VI) is weakly sorbed and hence, it is susceptible to
90 mobilization (Neal and Sposito, 1989; Goh and Lim, 2004; Goldberg et al., 2008). Nevertheless,
91 the potential transport of contaminants into the environment is poorly understood (Vengosh et al.,
92 2014; McLaughlin et al., 2016).
93
94 Balaba and Smart (2012) have demonstrated that flowback water is capable of leaching more As
95 and Se from Marcellus Shale than high-salinity or acidic solutions, and Wang et al. (2016) have
96 shown larger amounts of Fe, Ca, and As were mobilized at a lower solution pH. These studies
97 imply the significance of ionic strength and solution chemistry on trace metal mobilization.
98 Increasing ionic strength in subsurface solutions can reduce electrostatic repulsion and enhance
99 particle aggregation, which may inhibit As and Se sorption on mineral surfaces on soils due to
100 ion pairing and complexation with brine elements, thereby releasing them into groundwater
101 (Goldberg and Johnston, 2001; Goldberg et al., 2008; Fontenot et al., 2013). In addition,
102 mobilization of metal-laden colloids could be induced by hydrodynamic shear due to the high
103 flow rate of produced water in fractured media (e.g., 4-550 L h^{-1}) (Ziemkiewicz et al., 2014). The
104 presence of inorganic salts and surfactants in produced water may also influence the colloid
105 mobilization in soils, resulting in the colloidal-facilitated contaminant transport (Ryan and
106 Elimelech, 1996; Ma et al., 2016). It has been recently demonstrated that produced water could
107 mobilize model environmental colloids from sand grains due to steric repulsion by sorption of
108 organic compounds and cation exchange (Sang et al., 2014). The effects of produced water on
109 metal/metalloid transport in soils, which have more heterogeneous properties than sand, are still

unclear.

In view of the limited information available currently, this study is an investigation of the potential migration of metals, specifically As(V) and Se(VI), in the selected surface soils of shale regions under varying hydrogeochemical conditions, which may provide insight into the impact of accidental spills of produced water in the vicinity of fractured wells. The metal/metalloid transport behaviour is elucidated by HYDRUS-1D modelling (PC-PROGRESS), which numerically solves solute movement in saturated porous media based on advection-dispersion equations (Šimůnek et al., 2013). The transport parameters such as hydrodynamic dispersion coefficient, distribution coefficient, and immobile water content can reflect the influence of solution composition on flow paths and pore system in soils. This helps to understand the significance of temporal variations in the compositions of synthetic produced water at different stages of operation.

Material and methods

Soil sampling and synthetic produced water

Four types of surface soils were sampled from different sampling locations in Heilongjiang Province, China in order to investigate the importance of soil properties for the resultant metal/metalloid transport. They were sandy clay loam from Anda (46°04' N, 124°58' E), loamy sand from Bayan (46°26' N, 127°06' E), loam from Binxian (45°43' N, 127°28' E), and sandy loam Daqing (46°33' N, 125°01' E), respectively (Table 1). The sampling points are near Qingshankou formation in Songliao Basin, China, which also overlap with an elevated-arsenic-risk region (Rodriguez-Lado et al., 2013). The soils were sampled from the top 5 to 20 cm, and

133 then ground and sieved through 2 mm. Anda (AD) soil (pH 8.8) contained 21.0 mg g^{-1}
134 amorphous Fe and 25.3 mg g^{-1} total organic carbon (TOC). Bayan (BY) soil (pH 9.3) had the
135 largest amount of amorphous Fe (45.0 mg g^{-1}) and a comparable TOC content (24.8 mg g^{-1}),
136 while Binxian (BX) soil (pH 8.1) contained a relatively high content of amorphous Fe (38.7 mg
137 g^{-1}) but less TOC (10.2 mg g^{-1}). In contrast, Daqing (DQ) soil (pH 8.3) was comparatively low in
138 both contents of amorphous Fe (9.36 mg g^{-1}) and TOC (12.4 mg g^{-1}). As the amorphous Fe and
139 organic carbon content in soils provide major adsorption sites for arsenic as As(V) and selenium
140 as Se(VI) (Goldberg et al., 2008; Moreno-Jiménez et al., 2013), the metal mobilization may vary
141 with different soil characteristics (Table 1) and thus the four soils were studied in parallel. The
142 mobility of background As(V) and Se(VI) was tested by leaching in unbuffered deionized water
143 (Table S1, Supplementary Information).
144
145 The synthetic produced water was prepared according to the reported characteristics of samples
146 taken at Day 1, Day 14, and Day 90 as summarized in Table 2 (Hayes, 2009), which represented
147 significant temporal variation in solution composition, such as ionic strength and iron content, in
148 the field. The data were adopted from U.S. produced water as the relevant information was not
149 available in China. Anionic PAM ((-$CH_2CHCONH_2$-)n) (0.088% v/v), ethylene glycol
150 ($HOCH_2CH_2OH$) (0.043% v/v), and glutaraldehyde ($CH_2(CH_2CHO)_2$) (0.001%) were added as
151 commonly used fracturing additives. However, it should be noted that the additives listed in
152 Table 2 were not exhaustive, as the constituents in fracturing fluids can vary with geological
153 conditions and operation methods (information obtained from FracFocus database;
154 www.FracFocus.org). Although the concentrations of the organic additives will change over time,
155 they were kept at constant concentrations in this study in order to address the effects of high

ionic strength and TDS. Freshly collected wastewater samples from the field are needed to investigate the temporal effects imposed by organic additives in the future. To study the transport behaviour and assess the associated risks of heavy metals due to the spill and leakage of produced water near the ground surface, 100 μg L^{-1} concentrations of As(V) and Se(VI) (SPEX CertiPrep, Assurance Grade Standard Solution, USA) were spiked into synthetic produced water, because they are commonly associated with fracturing wastewater (Abualfaraj et al., 2014). Owing to accidental spills, the produced water may contaminate soil and groundwater and thereby raising toxicity concerns to humans and the environment (Chen et al., 2017; McLaughlin et al., 2016). In addition, the breakthrough of Sr and Fe was measured as they are also present in large quantities in the produced water.

Metal/metalloid transport in column experiments

The column experiments were undertaken to illustrate the impact of accidental spills of produced water recovered at different stages (i.e., Day 1, Day 14, and Day 90). Each column (15.4 mm dia., 61.55 mm depth) was packed with one soil sample at a bulk density of 1.34-1.37 g cm^{-3}, and placed with 8-μm filter papers (Grade 1, Whatman) at both ends. Preliminary experiments indicated that it was necessary to blend the soils with 50 wt% of acid-washed Ottawa quartz sand to maintain permeability and prevent clogging in the columns. Previous studies have also demonstrated the applicability of a mixture of quartz sand in the column experiments for investigating the pollutant transport in saturated porous media (Ryan and Gschwend, 1994; Yu et al., 2011; Sang et al., 2014). The pore volume (PV) of each column and the bulk density of each soil were calculated accordingly (AD: 1.70 g cm^{-3}; BY: 1.65 g cm^{-3}; BX: 1.62 g cm^{-3}; DQ: 1.65 g cm^{-3}) (Table 1). The soil columns were saturated with an upflow of background solution (10 mM

179 $NaNO_3$, pH 5.5) using a peristaltic pump at a steady pore water velocity of 10 ± 0.5 cm h^{-1},
180 which was similar to the infiltration rate of simulated acid rain (Hu et al., 2008).
181
182 After preconditioning for at least 20 PV, the columns were leached with 40 PV of Day 1, Day 14,
183 and Day 90 synthetic produced water (i.e., sorption phase), respectively. The flow was stopped
184 for 12 h (i.e., flow cessation), which could illustrate the significance of mass transfer limitations
185 that account for non-equilibrium processes and colloid release in saturated soil (Fritzsche et al.,
186 2011). Afterwards, the leaching of produced water was resumed for 20 PV to reach steady
187 condition. Then, the soils were desorbed by leaching with background solution for 20 PV (i.e.,
188 desorption phase), followed by a second 12-h flow cessation and additional desorption by 10 PV
189 of background solution. The effluent samples were continuously collected throughout the column
190 experiments, acidified with concentrated hydrochloric acid to pH less than 2, and stored at 4 °C.
191 Testing of the effluent samples did not distinguish between the colloidal and dissolved phases,
192 and only the total concentrations of the elements were used in the transport modelling, as
193 discussed later (Šimůnek et al., 2013). The total concentrations of As and Se were determined by
194 Atomic Absorption Spectrometry with vapour generation accessory (VGA-AAS, Agilent
195 VGA77, limit of detection 1 μg L^{-1}) while Fe and Sr were measured by AAS (limit of detection 1
196 mg L^{-1}). Arsenic speciation was analysed with disposable cartridges, and selenium speciation
197 was determined by VGA-AAS with the $NaBH_4$ as the reducing agent.
198
199 Lithium (50 mg L^{-1} $LiNO_3$, Sigma-Aldrich), which is weakly sorbed in our soils, was adopted as
200 a tracer in the column experiments (Sullivan et al., 2003; Fernàndez-Garcia et al., 2004; Pedretti
201 et al., 2013), as chloride and bromide were present as constituents of the produced water (Table

2), rendering them unsuitable as tracer elements. To examine the change of hydrogeological conditions, tracer breakthrough tests were conducted at three different stages: (i) upon preconditioning; (ii) at the end of leaching with produced water (sorption phase); and (iii) at the end of leaching with background solution (desorption phase), respectively. For each run, a 12-PV pulse of Li injection was followed by 24-PV desorption with background solution. The concentrations of Li in the collected effluent were analysed by AAS (limit of detection 0.1 mg L^{-1}). The breakthrough curves (BTCs) were constructed by plotting the relative concentration C/C_0 (effluent concentration/input concentration) against dimensionless time PV (pore volume), and then were modelled with equilibrium and two-region physical non-equilibrium transport equations using HYDRUS-1D version 4.16 (Šimůnek et al., 2013). The dispersion coefficients of the columns were obtained from the transport modelling of the tracer tests, which were used for the transport modelling of As(V), Se(VI), Sr, and Fe in the columns. Details of the transport equations and modelling can be found in the Supplementary Information and our previous studies (Tsang et al., 2006; 2007).

Results and Discussion

Significance of solution composition on metal/metalloid transport

A negligible amount of As(III) was found after column studies by the analysis of disposable cartridges. This observation was in agreement with the slow chemical kinetics of the reduction from As(V) to As(III) (Ascar et al., 2008), and As(V) was the predominant form in oxidizing produced water. Likewise, only Se(VI) was found in this study, which was the predominant form in alkaline soil and oxidized environment (Goh and Lim, 2004). The results for the BY soil are presented in Figure 1, which had the highest Fe and TOC content. The effluent concentrations of

As(V), Se(VI), Fe, and Sr showed a rapid breakthrough in less than 10 PV of sorption phase (Figure 1), and also a fast desorption within 15 PV of desorption phase in all produced water. It was interesting to note that even more rapid breakthroughs occurred with increasing ionic strength (*I*) in Day 14 and Day 90 solutions.

The two-region physical non-equilibrium model (Figure 1) generally fitted the measured data better than an equilibrium model (Figure S1). Comparable results were observed for the other three soils (Figure S2) despite their variations in Fe and TOC content. Additional tests with blending the soil samples with 20 wt% sand in the columns also displayed similar metal/metalloid transport in the four soil samples (Figure S3). Therefore, the results of this study indicated that solution compositions could play a predominant role in controlling the metal/metalloid transport, although the soil properties and mixture with sand are still important. It should be noted that although blending the soils with 20-50 wt% quartz sand helped to maintain permeability and prevent clogging in this study, the sand grains were observed to enhance the metal/metalloid breakthrough and reduce their adsorption onto the soils. For instance, the negatively charged surface on sand could enhance the transport of oxyanions (e.g., As(V) and Se(VI)) by increasing the repulsive force (Ryan and Elimelech, 1996).

The BTCs of As(V) and Se(VI) in Day 1 solution (pH 7.2, I = 0.35 M, Table 2) exhibited a long tailing during both sorption and desorption phases, and the extent of tailing was greater for the Se(VI). After the flow interruption and resumption, there was a remarkable decrease of the As(V) and Se(VI) concentrations during the adsorption phase of Day 1 solution (at about 55-60 PV), and a small increase during the desorption phase (at about 95-100 PV). This indicated the

248 significance of non-equilibrium transport behaviour because the flow interruptions allowed a
249 longer residence time for sorption/desorption to occur (Tsang et al., 2007; Zhang et al., 2013;
250 Fang et al., 2016), which was rate-limited probably due to the mass transfer between immobile
251 and mobile water regions (Brusseau et al., 1997). This was further investigated by means of
252 tracer tests in the subsequent section.
253
254 In contrast, long tailing and rebound upon flow interruption were notably less significant in Day
255 14 solution (pH 6.5, I = 2.49 M, Table 2), and almost negligible in Day 90 solution (pH 5.9, I =
256 4.10 M, Table 2). This signified a lesser extent of non-equilibrium transport behaviour, and
257 clearly indicated the important role of solution compositions on metal/metalloid transport. On
258 one hand, the addition of inorganic ions such as sodium, calcium, and chloride in the produced
259 water are known to be critical components for colloid mobilization (Ryan and Elimelech, 1996;
260 Sang et al., 2014), while on the other hand, the PAM used in the fracking fluids is also a
261 common soil conditioner that could enhance soil aggregation and inhibit colloid mobilization
262 (Seybold, 1994; Awad et al., 2013). At the elevated ionic strength, the produced water was less
263 likely to mobilize colloids due to more compressed electrical double layers, as well as increased
264 PAM adsorption on the soil by van der Waals forces (Seybold, 1994; Ryan and Elimelech, 1996;
265 Awad et al., 2016). Hence, the results of this study suggested that the presence of extremely high
266 ionic strength in Day 14 and Day 90 solutions could reduce the likelihood of non-equilibrium
267 transport behaviour. This was possibly because of the change in hydrogeological conditions as
268 indicated by the variations in the fraction of sorption sites in contact with mobile water (f_{mo}) and
269 immobile water content (θ_{im}) in Table 3 and Table S2.
270

In comparison, the transport of Sr and Fe displayed rapid breakthrough, insignificant rebound upon flow interruptions, and undetectable tailings for all solutions (Figure 1) and soils (Figure S2). However, some overshoot of effluent concentrations, i.e., $C/C_0 > 1$, was observed probably due to rapid sorption of Fe and Sr followed by ion exclusion during the leaching of produced water.

Change of hydrogeological conditions due to leaching of produced water

Figure 2 provides a comparison of the lithium BTCs in BY soil at different stages of leaching. Prior to leaching of Day 1 solution (Figure 2a), both the simulations of the equilibrium and two-region physical non-equilibrium models were in close agreement with the lithium BTCs. In contrast, after the leaching of produced water (Figure 2b), the experimental data were more closely represented by the physical non-equilibrium model, particularly for the early appearance of Li and the asymmetry of the BTC. Therefore, the tracer tests confirmed the absence of physical non-equilibrium condition in background solution, but the introduction of produced water resulted in a substantial change in the flow characteristics and transport channels. This change of the soil structure may be related to the compressed electrical double layers of mineral oxides and soil particles/colloids, and PAM-induced particle aggregation at the elevated ionic strength (Wu et al., 2012). The saturation capacity of PAM is known to increase significantly with increasing TDS, and fine soils also enhance its sorption while organic matter has a negative effect (Lu et al., 2002). Similar trends were also found in the other three soils regardless of variations in the soil texture and properties (Figure S4).

Interestingly, after desorption by background solution (Figure 2c), the simulations of the

294 equilibrium model resembled those of the physical non-equilibrium model, both of which
295 described the experimental data reasonably well (except AD soil in Figure S4). The variations of
296 θ_{im} and first-order mass transfer coefficient (α_s) were also evident at different stages of leaching
297 in BY soil (Table 4) and the other three soils (Table S3). These values consistently decreased in
298 all soils when the conditions changed from preconditioning with background solution to post-
299 leaching of produced water, whereas they increased again at the end of desorption by
300 background solution. The changes of parameter values corroborated the curve fitting of the
301 model simulations. Such a reversible change of the flow characteristics after leaching with
302 background solution may indicate that the expanding electrical double layers at a much lower
303 electrolyte concentration (compared to that of produced water) may detach the anionic PAM
304 from the soil surfaces (Seybold, 1994; Ryan and Elimelech, 1996). An increased turbidity in the
305 effluent was observed at the beginning of leaching with background solution. The effects of
306 anionic PAM sorption by soils deserve more investigation in the future as its sorption could
307 influence the mobility of oxyanions.
308
309 *Sorption/desorption of As(V) and Se(VI) in produced water*
310 The transport of As(V) and Se(VI) may be affected also by sorption onto iron oxyhydroxides in
311 soil, which varied with solution ionic strength (Peak and Sparks, 2002; Xu et al., 2009;
312 Vithanage et al., 2013). As indicated by area integration of the BTCs, the sorption of As(V) on
313 BY soil was comparatively less in Day 14 solution while the sorption of Se(VI) increased with
314 increasing ionic strength. Similar changes were observed with the other three soil samples
315 (Figure 3a&b). A previous study has suggested an increasing As(V) sorption on amorphous
316 oxides with decreasing solution pH and increasing ionic strength (Goldberg and Johnston, 2001).

Besides, the pH values of Day 14 (pH 6.5) and Day 90 (pH 5.9) solutions were lower than that of Day 1 (pH 7.2) solution (Table 2), in which the soil surface would be more positively charged and conducive to the sorption of oxyanions (e.g., arsenate and selenate) as the point of zero charge of amorphous iron oxide is about pH 8 (Dzombak and Morel, 1990). These previous findings would suggest a prediction of an increasing sorption in our tests from Day 1 to Day 90 solutions.

The discrepancy between the results and the prediction could be explained by the changes of the electrostatic potential in the plane of adsorption. For soils displaying variable charge, the capacity of anion sorption at different ionic strengths would approach the same value at the pH of the point of zero salt effect (PZSE). At a pH below the PZSE the soil exhibited a positively charged plane of adsorption for the anions, in which an increasing ionic strength would accumulate more counter-ions (Barrow and Ellis, 1986; Bolan et al., 1986; Xu et al., 2009). Hence, the sorption of As(V) and Se(VI) was reduced with increasing ionic strength as illustrated in Figure S5, whereas the behaviour was the reverse above the PZSE. Therefore, the results of this study implied that the PZSE of the four soils probably lied above the pH values of produced water (Figure S5), accounting for the observed changes in As(V) and Se(VI) sorption (Figure 3a&b).

After the subsequent leaching by background solution, As(V) had minimal desorption from all soils (Figure 3c), i.e., less than 5% of the sorbed amount (except desorption from DQ soil after the leaching of Day 1 and Day 14 solutions). This could be explained by the DQ soil having the least amount of amorphous iron content, which has been found important for specific sorption of

As(V) (Goldberg and Johnston, 2001; Dixit and Hering, 2003; Wilson et al., 2010). In comparison, it was evident that Se(VI) desorbed from the soils easily after the leaching of Day 1 solution (Figure 3d), which is consistent with other studies that have demonstrated its weak sorption in soils. However, the significant reduction of desorption after the leaching of Day 14 and Day 90 solutions might be attributed to the continuum of sorption mechanisms of oxyanions. The sorption of Se(VI) could take place via a varying proportion of outer-sphere and inner-sphere surface complexation, which would primarily depend on the environmental conditions such as ionic strength, solution pH, and surface loading on the soils. The results implied that more strongly bound complexes could be formed between Se(VI) and soil surface at a high ionic strength, which was in agreement with previous findings (Neal and Sposito, 1989; Peak and Sparks, 2002). Therefore, in summary, the transport and sorption/desorption of As(V) and Se(VI) was both pH- and ionic strength-dependent.

It should be noted that redox potential and microbial-mediated transformation can also affect metal/metalloid speciation and their fate. However, the redox potential of the effluent samples remained stable under an oxidizing condition (~220 mV) with little fluctuation throughout the column experiments in this study. Besides, it has been shown that ethylene glycol did not degrade in a biotic reactor with agricultural topsoil and synthetic fracking fluids over 180 days in the presence of glutaraldehyde as a biocide (McLaughlin et al., 2016). Therefore, it is anticipated that the microbial-induced reduction of redox potential imposed negligible influence on the observed metal/metalloid transport in this study.

According to the metal mobility and transport behaviour, it may be possible to give an insight

363 into the environmental setback distance, i.e., horizontal distance from the perimeter of
364 contamination to the nearest adjacent property line that is required for protecting public health
365 (Davies et al., 2004; Hijnen et al., 2005; Pang et al., 2005). The setback distance is positively
366 related to soil density and the distribution coefficient (K_d) of the non-equilibrium transport model
367 (Rogers et al., 2015). The values of K_d for As and Se were the largest in Day 90 solution (Table 3
368 and Table S2), which corroborated the results of area integration of the BTCs (Figure 3). Yet, it
369 should be noted that the estimation of setback distance should take into account the
370 compositional variation of on-site produced water and the corresponding transport simulations.
371 For example, the use of biocide and presence of high salt concentrations during fracking could
372 inhibit the microbial activities responsible for contaminant attenuation, and consequently
373 increase the distance that the contaminants are transported (McLaughlin et al., 2016). Therefore,
374 a comprehensive evaluation of concerned inorganic and organic contaminants as well as
375 hydrogeological conditions is needed to derive a site-specific setback distance.
376
377 **Conclusions**
378 This study has investigated potential interactions between contaminated produced water and soils
379 representative of shale gas areas in Northeast China. By means of column tests and transport
380 modelling of As(V) and Se(VI) breakthroughs, the results indicated non-equilibrium transport
381 behaviour in Day 1 and Day 14 solutions, while the higher ionic strength of Day 90 solution led
382 to soil aggregation that altered flow transport channels. A rapid desorption of the
383 metals/metalloids implied a potential contamination risk to the surface/ground water resources.
384 The influence of produced water on hydrogeological conditions was demonstrated by the change
385 of tracer breakthroughs before and after leaching of the solutions. However, the interaction

386 between PAM in the produced water and soil surfaces was found to be reversible indicating its
387 dependence on the local conditions. In addition, the results have shown that solution chemistry,
388 in particular the pH value and ionic strength, has a major influence on the sorption and
389 desorption of As(V) and Se(VI) in sandy and loamy soils. Future work on sorption mechanisms
390 is recommended to complement the hydrogeological aspects revealed by this study.
391 Understanding the observed metal/metalloid transport behaviour in the produced water would
392 help us derive an environmental setback distance for risk assessment and management.
393
394 **Acknowledgements**
395 This work was supported by the National Natural Science Foundation of China (21407121);
396 Hong Kong Research Grants Council (PolyU 538613 and 15222115]; and Open Project of State
397 Key Laboratory of Urban Water Resource and Environment (HCK201209).
398
399 **References**
400 Abualfaraj, N., Gurian, P.L., and Olson, M.S., 2014. Characterization of Marcellus shale
401 flowback water. Environ. Eng. Sci. 31, 514-524.
402 Ascar, L., Ahumada, I., Richter, P., 2008. Influence of redox potential (Eh) on the availability of
403 arsenic species in soils and soils amended with biosolid. Chemosphere 72, 1548-1552.
404 Awad, Y.M., Blagodatskaya, E., Ok, Y.S., Kuzyakov, Y., 2013. Effects of polyacrylamide,
405 biopolymer and biochar on the decomposition of ^{14}C-labelled maize residues and on their
406 stabilization in soil aggregates. Eur. J. Soil Sci. 64, 488–499.
407 Awad, Y.M., Lee, S.S., Ok, Y.S., Kuzyakov, Y., 2016. Effects of biochar and polyacrylamide on
408 decomposition of soil organic matter and ^{14}C-labeled alfalfa residue. J. Soils Sediments, in press.

409 Balaba, R.S.; Smart, R.B., 2012. Total arsenic and selenium analysis in Marcellus shale, high-
410 salinity water, and hydrofracture flowback wastewater. Chemosphere 89(11), 1437-1442.
411 Barbot, E., Vidic, N. S., Gregory, K. B., Vidic, R. D., 2013. Spatial and temporal correlation of
412 water quality parameters of produced waters from Devonian-age shale following hydraulic
413 fracturing. Environ. Sci. Technol. 47 (6), 2562-2569.
414 Barrow, N.J., Ellis, A.S., 1986. Testing a mechanistic model. V. The points of zero salt effect for
415 phosphate retention, for zinc retention and for acid/alkali titration of a soil. J. Soil Sci. 37, 303-
416 310.
417 Bolan, N.S., Syers, J.K., Tillman, R.W., 1986. Ionic strength effects on surface charge and
418 adsorption on phosphate and sulphate by soils. J. Soil Sci. 37, 379-388.
419 Brusseau, M.L., Hu, Q., Srivastava, R., 1997. Using flow interruption to identify factors causing
420 nonideal contaminant transport. J. Contam. Hydrol. 24, 205-219.
421 Chen, S.S., Sun, Y., Tsang, D.C.W., Graham, N.J.D., Ok, Y.S., Feng, Y., Li, X.D., 2017.
422 Potential impact of flowback water from hydraulic fracturing on agricultural soil quality:
423 Metal/metalloid bioaccessibility, Microtox bioassay, and enzyme activities. Sci. Total Environ.
424 579, 1419-1426.
425 China's State Council http://english.gov.cn/policies/ accessed on 21 Mar 2015.
426 Davies, C.M., Ferguson, C.M., Kaucner, C., Krogh, M., Altavilla, N., Deere, D.A., Ashbolt, N.J.,
427 2004. Dispersion and transport of Cryptosporidium oocysts from fecal pats under simulated
428 rainfall events. Appl. Environ. Microbiol. 70, 1151-1159.
429 Dixit, S.; Hering, J.G., 2003. Comparison of Arsenic (V) and Arsenic (III) Sorption onto Iron
430 Oxide Minerals: Implications for Arsenic Mobility. Environ. Sci. Technol. 37, 4182-4189.
431 Dzombak, D., Morel, F., 1990. Surface Complexation Modeling: Hydrous Ferric Oxide; John

Wiley and Sons, New Jersey.

Fang, S., Tsang, D.C.W., Zhou, F., Zhang, W., Qiu, R., 2016. Stabilization of cationic and anionic metal species in contaminated soils using sludge-derived biochar. Chemosphere 149, 363-271.

Fernàndez-Garcia, D., Illangasekare, T.H., Rajaram, H., 2004. Conservative and sorptive forced-gradient and uniform flow tracer tests in a three-dimensional laboratory test aquifer. Water Resour. Res. 40, W10103.

Ferrar, K.J., Michanowicz, D.R., Christen, C.L., Mulcahy, N., Malone, S.L., and Sharma, R.K., 2013. Assessment of effluent contaminants from three facilities discharging Marcellus shale wastewater to surface waters in Pennsylvania. Environ. Sci. Technol. 47, 3472-3481.

Fontenot, B.E., Hunt, L.R., Hildenbrand, Z.L., Carlton Jr., D.D., Oka, H., Walton, J.L., Hopkins, D., Osorio, A., Bjorndal, B., Hu, Q.H., and Schug, K.A., 2013. An evaluation of water quality in private drinking water wells near natural gas extraction sites in the Barnett shale formation. Environ. Sci. Technol. 47, 10032-10040.

FracFocus, 2016. What chemicals are used. https://fracfocus.org/chemical-use/what-chemicals-are-used (accessed 15.03.20).

Fritzsche, A., Rennert, T., Totsche, K.U., 2011. Arsenic strongly associates with ferrihydrite colloids formed in a soil effluent. Environ. Pollut. 159, 1398-1405.

Goh, K.H., Lim, T.T., 2004. Geochemistry of inorganic arsenic and selenium in a tropical soil: effect of reaction time, pH, and competitive anions on arsenic and selenium adsorption. Chemosphere 55, 849-859.

Goldberg, S., Hyun, S., Lee, L.S., 2008. Chemical modeling of arsenic (III, V) and selenium (V) adsorption by soils surrounding ash disposal facilities. Vadose Zone J. 7(4), 1231-1238.

455 Goldberg, S., Johnston, C.T., 2001. Mechanisms of arsenic adsorption on amorphous oxides
456 evaluated using macroscopic measurements, vibrational spectroscopy, and surface complexation
457 modeling. J. Colloid Interface Sci. 234, 204-216.
458 Gradient, 2012. Human Health Risk Evaluation for Hydraulic Fracturing Fluid Additives.
459 https://yosemite.epa.gov/sab/sabproduct.nsf/3D73316595F846C185257C2400686964/$File/Gra
460 dient+Human+Health+Risk+Evaluation.pdf
461 Gregory, K.B., Vidic, R.D., and Dzombak, D.A., 2011. Water management challenges associated
462 with the production of shale gas by hydraulic fracturing. Elements 7, 181-186.
463 Haluszczak, L., Rose, A., Kump, L., 2013. Geochemical evaluation of flowback brine from
464 Marcellus gas wells in Pennsylvania, USA. Appl. Geochem. 28, 55-61.
465 Hayes, T., 2009. Sampling and Analysis of Water Streams Associated with the Development of
466 Marcellus Shale Gas. Final report prepared for Marcellus Shale Coalition, Gas Technology
467 Institute, Des Plaines, IL 60018.
468 Hijnen, W.A.M., Brouwer-Hanzens, A.J., Charles, K.J., Medema, G.J., 2005. Transport of MS2
469 phage, Escherichia coli, Clostridium perfringens, Cryptosporidium parvum, and giardia
470 intestinalis in a gravel and a sandy soil. Environ. Sci. Technol. 39, 7860-7868.
471 Hu, S., Chen, X., Shi, J., Chen, Y., Lin, Q., 2008. Particle-facilitated lead and arsenic transport in
472 abandoned mine sites soil influenced by simulated acid rain. Chemosphere, 71, 2091-2097.
473 Jackson, R.E., Gorody, A.W., Mayer, B., Roy, J.W., Ryan, M.C., and Van Stempvoort, D.R.,
474 2013. Groundwater protection and unconventional gas extraction: The critical need for field-
475 based hydrogeological research. Groundwater 51(4), 488-510.
476 Kargbo, D. M.; Wilhelm, R. G.; Campbell, D. J. Natural gas plays in the Marcellus Shale:
477 challenges and potential opportunities. Environ. Sci. Technol. 2010, 44 (15), 5679−5684.

478 Kim, E.J., Yoo, J.C., Baek, K., 2014. Arsenic speciation and bioaccessibility in arsenic-
479 contaminated soils: Sequential extraction and mineralogical investigation. Environ. Pollut. 186,
480 29-35.
481 King, G. E. Hydraulic Fracturing 101: What Every Representative, Environmentalist, Regulator,
482 Reporter, Investor, University Researcher, Neighbor and Engineer Should Know About
483 Estimating Frac Risk and Improving Frac Performance in Unconventional Gas and Oil Wells;
484 Woodlands, TX, 2012; DOI 10.2118/152596-MS.
485 Kondash, A.J., Warner, N.R., Lahav, O., Vengosh, A., 2013. Radium and barium removal
486 through blending hydraulic fracturing fluids with acid mine drainage. Environ. Sci. Technol. 48,
487 1334-1342.
488 Lauer, N.E., Harkness, J.S., Vengosh, A., 2016. Brine spills associated with unconventional oil
489 development in North Dakota. Environ. Sci. Technol. 50, 5389-5397.
490 Lu, J.H., Wu, L., Letey, J., 2002. Effects of soil and water properties on anionic polyacrylamide
491 sorption. Soil Sci. Soc. Am. J. 66, 578-584.
492 Ma, J., Guo, H., Lei, M., Wan, X., Zhang, H., Feng, X., Wei, R., Tian, L., Han, X., 2016.
493 Blocking effect of colloids on arsenate adsorption during co-transport through saturated sand
494 columns. Environ. Pollut. 213, 638-647.
495 McLaughlin, M.C., Borch, T., Blotevogel, J., 2016. Spills of hydraulic fracturing chemicals on
496 agricultural biodegradation, sorption, and co-contaminant interactions. Environ. Sci. Technol. 50,
497 6071-6078.
498 Milligan, C., Reddy, K.J., 2007. Monitoring of groundwater contamination by trace elements
499 from CBNG disposal ponds across the Powder River Basin, Wyoming: Proceedings of a Joint
500 Conference of American Society of Mining and Reclamation 24th Annual National Conference,

p. 520-527.

Moore, C.W., Zielinska, B., Petron, G., Jackson, R.B., 2014. Air impacts of increased natural gas acquisition, processing, and use: A critical review. Environ. Sci. Technol. 48, 8349-8359.

Moreno-Jiménez, E., Clemente, R., Mestrot, A., Meharg, A.A., 2013. Arsenic and selenium mobilisation from organic matter treated mine spoil with and without inorganic fertilisation. Environ. Pollut. 173, 238-244.

Neal, R.H., Sposito, G., 1989. Selenate adsorption on alluvial soils. Soil Sci. Soc. Am. J. 53, 70–74.

Nelson, A.W., May, D., Knight, A.W., Eitrheim, E.S., Mehrhoff, M., Shannon, R., Litman, R., Schultz, M.K., 2014. Matrix complications in the determination of radium levels in hydraulic fracturing flowback water from Marcellus shale. Environ. Sci. Technol. Lett. 1, 204-208.

Pang, L., Close, M., Goltz, M., Noonan, M., Sinton, L., 2005. Filtration and transport of Bacillus subtilis spores and the F-RNA phage MS2 in a coarse alluvial gravel aquifer: Implications in the estimation of setback distances. J. Contam. Hydrol. 77, 165-194.

Parnell, J., Brolly, C., Spinks, S., Bowden, S. 2016. Selenium enrichment in Carboniferous Shales, Britain and Ireland: Problem or opportunity for shale gas extraction? Appl. Geochem. 66, 82-87.

Peak, D., Sparks, L., 2002. Mechanisms of selenite adsorption on iron oxides and hydroxides. Environ. Sci. Technol. 36, 1460-1466.

Pedretti, D., Fernàndez-Garcia, D., Bolster, D., Sanchez-Vila, X., 2013. On the formation of breakthrough curves tailing during convergent flow tracer tests in three-dimensional heterogeneous aquifers. Water Resour. Res. 49, 1-17.

Phan, T.T., Capo, R.C., Stewart, B.W., Graney, J.R., Johnson, J.D., Sharma, S., Toro, J. 2015.

524 Trace metal distribution and mobility in drill cuttings and produced waters from Marcellus Shale
525 gas extraction: Uranium, arsenic, barium. Appl. Geochem. 60, 89-103.
526 Puls, R.W., Powell, R.M., 1992. Transport of Inorganic Colloids through Natural Aquifer
527 Material: Implications for Contaminant Transport. Environ. Sci. Technol. 26, 614-621.
528 Rodriguez-Lado, L., Sun, G., Berg, M., Zhang, Q., Xue, H. B., Zheng, Q. M., Johnson, C. A.,
529 2013. Groundwater arsenic contamination throughout China. Science 341 (6148), 866-868.
530 Rogers, J.D., Burke, T.L., Osborn, S.G., Ryan, J.N., 2015. A framework for identifying organic
531 compounds of concern in hydraulic fracturing fluids based on their mobility and persistence in
532 groundwater. Environ. Sci. Technol. Lett. 2, 158-164.
533 Ryan, J.N., Elimelech, M., 1996. Review: Colloid mobilization and transport in groundwater.
534 Colloids Surfaces A: Physicochem. Eng. Aspects 107, 1-56.
535 Ryan, J.N., Gschwend, P.M., 1994. Effect of solution chemistry on clay colloid release from an
536 iron oxide-coated aquifer sand. Environ. Sci. Technol. 28, 1717-1726.
537 Sang, W., Stoof, C.R., Zhang, W., Morales, V.L., Gao, B., Kay, R.W., Liu, L., Zhang, Y.,
538 Steenhuis, T.S., 2014. Effect of hydrofracking fluid on colloid transport in the unsaturated zone.
539 Environ. Sci. Technol. 48, 8266-8274.
540 Seybold, C.A., 1994. Polyacrylamide review: Soil conditioning and environmental fate.
541 Commun. Soil Sci. Plant Anal. 25, 2171-2185.
542 Šimůnek, J., Šejna, M., Saito, H., Sakai, M., van Genuchten, M. Th., 2013. The HYDRUS-1D
543 software package for simulating the one-dimensional movement of water, heat, and multiple
544 solutes in variably-saturated media, version 4.17. HYDRUS software series 3, Department of
545 Environmental Sciences, University of California Riverside, Riverside, California, USA; 2013.
546 342 pages.

547 Sullivan, E.J., Reimus, P.W., Counce, D.A., 2003. Transport of a reactive tracer in saturated
548 alluvium described using a three-component cation-exchange model. J. Contam. Hydrol. 62,
549 675-694.
550 Swarthout, R.F., Russo, R.S., Zhou, Y., Miller, B.M., Mitchell, B., Horsman, E., Lipsky, E.,
551 McCabe, D.C., Baum, E., Sive, B.C., 2015. Impact of Marcellus Shale natural gas development
552 in southwest Pennsylvania on volatile organic compound emissions and regional air quality.
553 Environ. Sci. Technol. 49, 3175-3184.
554 Tollefson, J., 2013. China slow to tap shale-gas bonanza. Nature 494 (7437), 294.
555 Tsang, D.C.W., Lo, I.M.C., 2006. Competitive Cu and Cd sorption and transport in soils: A
556 combined batch kinetics, column and sequential extraction study. Environ. Sci. Technol. 40,
557 6655-6661.
558 Tsang, D.C.W., Zhang, W., Lo, I.M.C., 2007. Modeling cadmium transport in soils using
559 sequential extraction, batch and miscible displacement experiments. Soil Sci. Soc. Am. J. 71,
560 674-681.
561 US EIA, 2013. Annual Energy Outlook for 2013. U.S. Energy Information Administration:
562 Washington DC, http://www.eia.gov/ forecasts/aeo/.
563 US EPA, 2009. Drinking Water Contaminants and their MCLs. Water.epa.
564 gov/drink/contaminants/.
565 US EPA, 2016. Unconventional oil and gas extraction effluent guidelines.
566 https://www.epa.gov/eg/unconventional-oil-and-gas-extraction-effluent-guidelines
567 Vengosh, A., Jackson, R.B., Warner, N., Darrah, T.H., Kondash, A., 2014. A critical review of
568 the risks to water resources from unconventional shale gas development and hydraulic fracturing
569 in the United States. Environ. Sci. Technol. 48, 8334-8348.

570 Vidic, R., Brantley, S., Vandenbossche, J., Yoxtheimer, D., and Abad, J., 2013. Impact of shale
571 gas development on regional water quality. Science 340, 12350091-12350099.
572 Vithanage, M., Rajapaksha, A.U., Dou, X., Bolan, N.S., Yang, J.E and Ok, Y.S. 2013. Surface
573 complexation modeling and spectroscopic evidence of antimony adsorption on iron-oxide-rich
574 red earth soils. J. Colloid Interface Sci. 406, 217-224.
575 Wang, L., Burns, S., Giammar, D.E., Fortner, J.D., 2016. Element mobilization from Bakken
576 shales as a function of water chemistry. Chemosphere 149, 286-293.
577 Warner, N.R., Christie, C.A., Jackson, R.B., and Vengosh, A., 2013. Impacts of shale gas
578 wastewater disposal on water quality in Western Pennsylvania. Environ. Sci. Technol. 47,
579 11849-11857.
580 Wilson, S.C., Lockwood, P.V., Ashley, P.M., Tighe, M., 2010. The chemistry and behaviour of
581 antimony in the soil environment with comparisons to arsenic: A critical review. Environ. Pollut.
582 158, 1169-1181.
583 Wu, L., Ok, Y.S., Xu, X.L., Kuzyakov, Y. 2012. Effects of anionic polyacrylamide on maize
584 growth: a short term 14C labelling study. Plant and Soil 350, 311-322.
585 Xu, R., Wang, Y., Tiwari, D., Wang, H., 2009. Effect of ionic strength on adsorption of As(III)
586 and As(V) on variable charge soils. J. Environ. Sci. 21, 927-932.
587 Yu, C., Gao, B., Munoz-Carpena, R., Tian, Y., Wu, L., Perez-Ovilla, O., 2011. A laboratory
588 study of colloid and solute transport in surface runoff on saturated soil. J. Hydrol. 402, 159-164.
589 Zhang, W., Tsang, D.C.W., Chen, H., Huang, L., 2013. Remediation of an electroplating
590 contaminated soil by EDTA flushing: Chromium release and soil dissolution. J. Soil. Sediment.
591 13, 354-363.
592 Ziemkiewicz, P.F., He, T., 2015. Evolution of water chemistry during Marcellus Shale gas

593 development: A case study in West Virginia. Chemosphere 134, 224-231.
594 Ziemkiewicz, P.F., Quaranta, J.D., Darnell, A.D., Wise, R., 2014. Exposure pathways related to
595 shale gas development and procedures for reducing environmental and public risk. J. Nat. Gas
596 Sci. Eng. 16, 77-84.
597 Zou, C., Dong, D., Wang, S., Li, J., Li, X., Wang, Y., Li, D., Cheng, K., 2010. Geological
598 characteristics and resource potential of shale gas in China. Petrol. Explor. Develop., 37, 641-
599 653.

Insights into the Subsurface Transport of As(V) and Se(VI) in Produced Water from Hydraulic Fracturing Using Soil Samples from Qingshankou Formation, Songliao Basin, China

Season S. Chen[1], Yuqing Sun[1,2], Daniel C.W. Tsang[1,*], Nigel J.D. Graham[2], Yujie Feng[3,*], Yong Sik Ok[4], Xiang-dong Li[1]

List of Figures

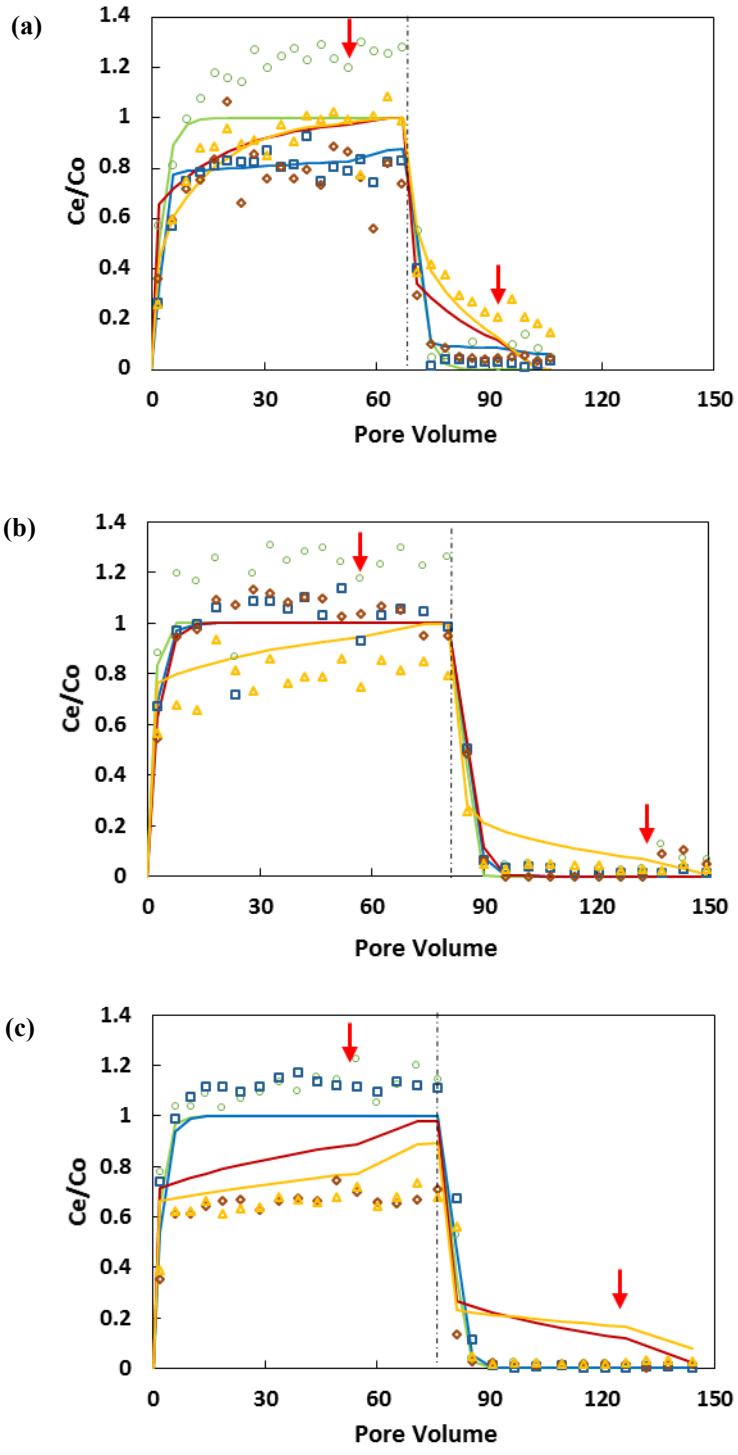

Figure 1. Breakthrough curves of metal/metalloid transport in BY soil: (a) Day 1 solution; (b) Day 14 solution; (c) Day 90 solution (experimental data: ◇ As(V), △ Se(VI), □ Sr, ○ Fe; two-region physical nonequilibrium model simulation: —As(V), —Se(VI), —Sr, —Fe; the dashed lines indicated end of sorption phase, and the arrows indicated flow interruptions during sorption phase and desorption phase, respectively).

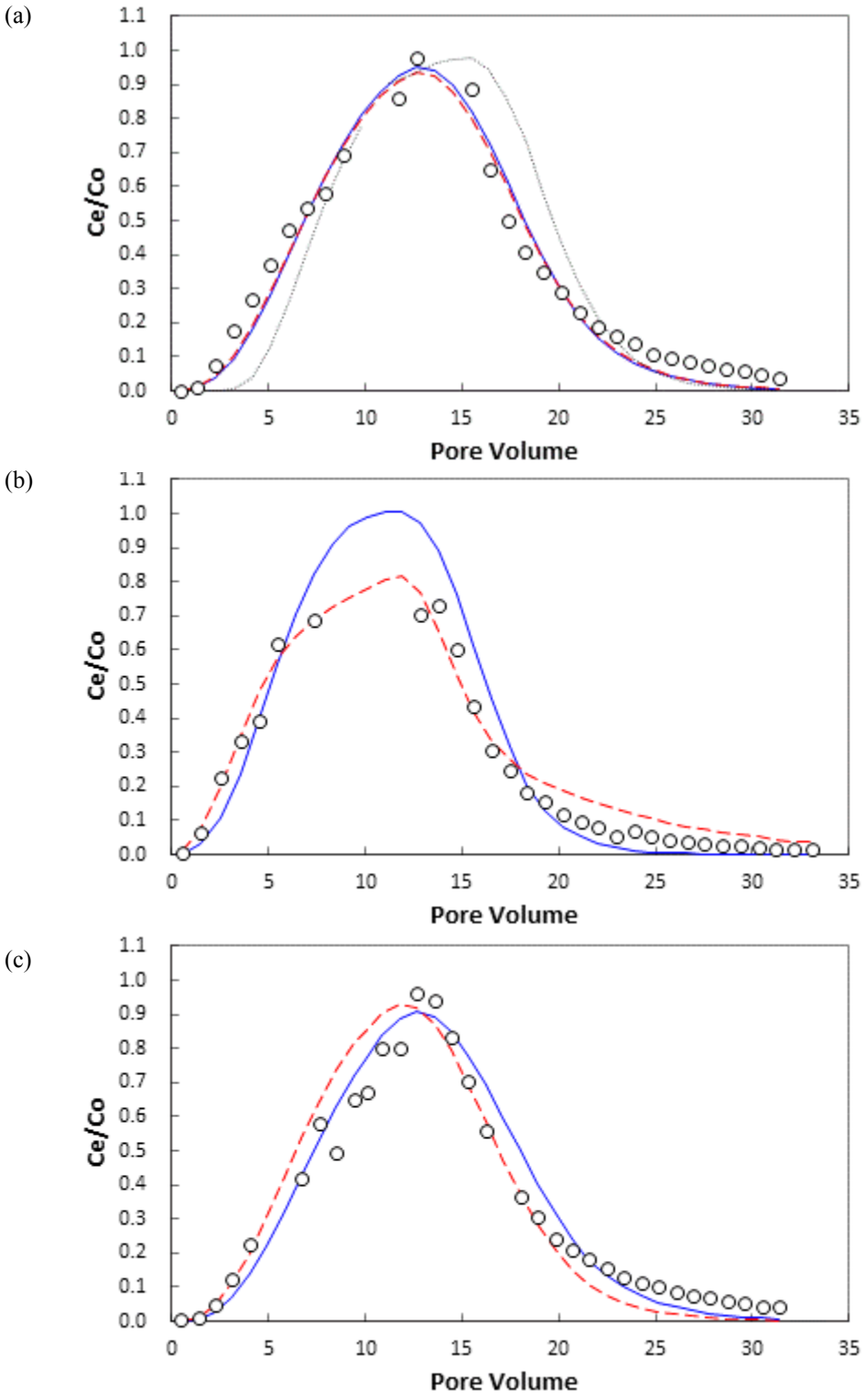

Figure 2. Breakthrough curves of lithium tracer in BY soil: (a) upon preconditioning with background solution; (b) at the end of leaching of Day 1 solution; and (c) at the end of desorption by background solution (○ experimental data; —— equilibrium model simulation; - - - - two-region physical nonequilibrium model simulation; ..... direct simulation).

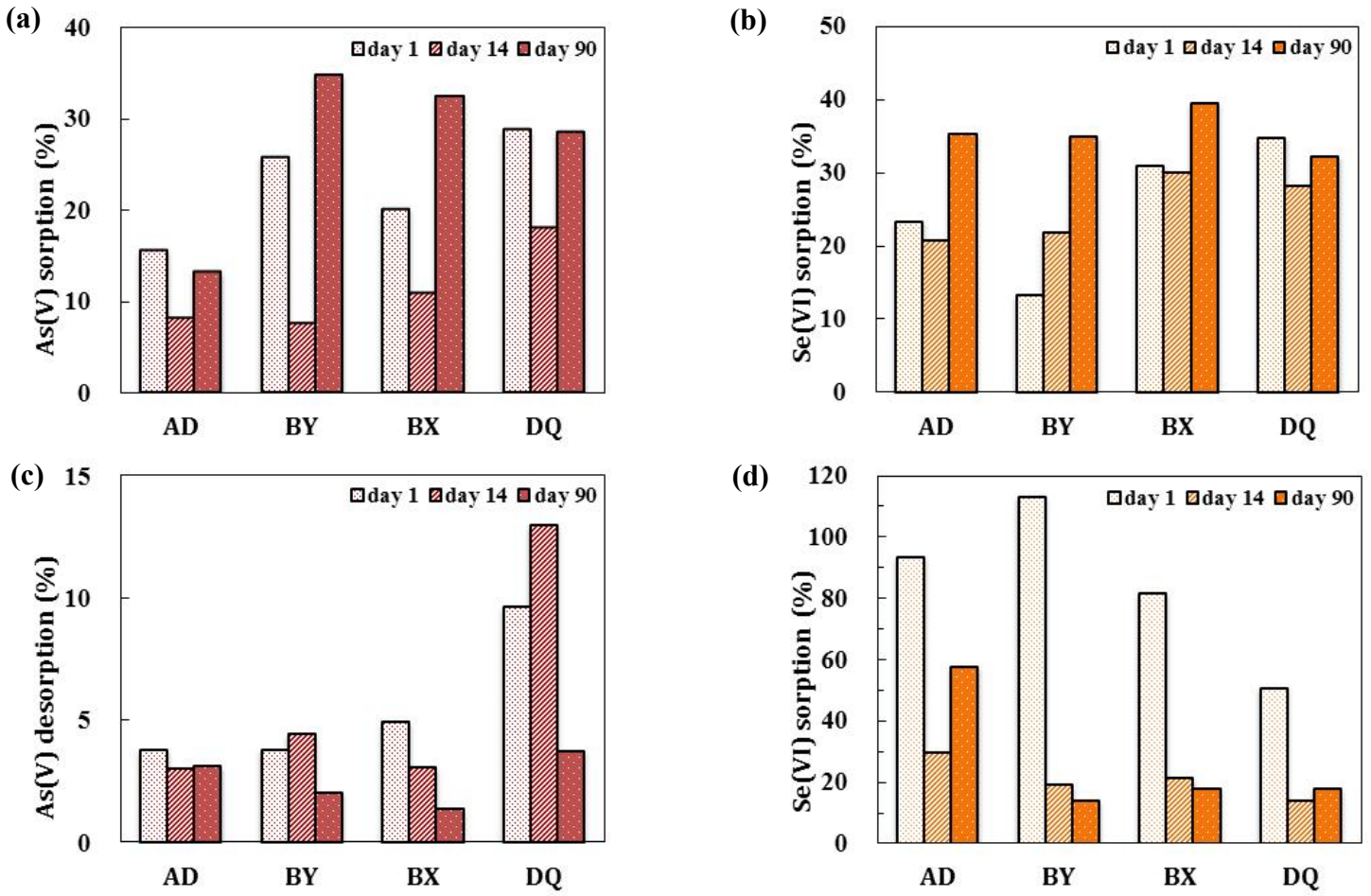

Figure 3. Sorption (a&b) and desorption (c&d) of As(V) and Se(VI) during the leaching of produced water.

Insights into the Subsurface Transport of As(V) and Se(VI) in Produced Water from Hydraulic Fracturing Using Soil Samples from Qingshankou Formation, Songliao Basin, China

Season S. Chen[1], Yuqing Sun[1,2], Daniel C.W. Tsang[1,*], Nigel J.D. Graham[2], Yujie Feng[3,*], Yong Sik Ok[4], Xiang-dong Li[1]

List of Tables

Table 1. Selected physico-chemical properties of the four surface soils in the Qingshankou shale region.

Soil	AD	BY	BX	DQ
Bulk density (g cm^{-3})	1.70	1.65	1.62	1.65
pH	8.8	9.3	8.1	8.3
Soil texture	Sandy clay loam	Loamy sand	Loam	Sandy loam
TOC (mg g^{-1}) [a]	25.3	24.8	10.2	12.4
CEC (cmol kg^{-1}) [b]	10.3	14.2	16.8	8.90
Fe (mg g^{-1}) [c]	21.0	45.0	38.7	9.36
Al (mg g^{-1}) [c]	32.0	24.9	20.4	9.63
Mn (mg g^{-1}) [c]	1.24	7.67	4.90	0.46
Si (mg g^{-1}) [c]	10.7	21.8	15.2	6.94

[a] total organic carbon;
[b] cation exchange capacity;
[c] extraction by ammonium oxalate at pH 3.

Table 2. Composition of the produced water at different stages of hydraulic fracturing process.

Produced Water	Day 1 (mg L^{-1})	Day 14 (mg L^{-1})	Day 90 (mg L^{-1})
Calcium	676	11050	18450
Barium	387	1835	2135
Magnesium	121	938	1700
Sodium	6015	31750	43700
Chloride	8410	79000	123500
Bromide	87.9	708.5	1175
Iron(III)	19.5	74.9	117
Strontium	156.5	3320	3140
Boron	8.1	16.4	17.8
Anionic Polyacrylamide	0.088% (v/v)	0.088% (v/v)	0.088% (v/v)
Ethylene glycol	0.043 (v/v)	0.043 (v/v)	0.043 (v/v)
Glutaraldehyde	0.001% (v/v)	0.001% (v/v)	0.001% (v/v)
Arsenic(V)	0.1	0.1	0.1
Selenium(VI)	0.1	0.1	0.1
pH	7.2	6.5	5.9
Ionic strength (M)	0.35	2.49	4.10

Table 3. Parameter values of the two-region physical nonequilibrium transport simulations in BY soil.

		Parameters					
		D (cm^2 min^{-1}) [a]	f_{mo} [b]	θ_{im} [c]	α_s (min^{-1}) [d]	K_d (cm^3 g^{-1}) [e]	R^2
Day 1	As(V)	0.206	0.00	0.29	1.76	3.44	0.92
	Se(VI)		0.28	0.35	2.47	4.72	0.94
	Fe		0.65	0.05	2.88	1.73	0.98
	Sr		0.08	0.35	0.81	22.28	0.98
Day 14	As(V)	0.221	0.34	0.34	11.89	1.28	0.99
	Se(VI)		0.23	0.35	0.93	3.51	0.97
	Fe		1.00	0.02	1.33	1.02	0.98
	Sr		0.86	0.35	2.94	1.24	0.97
Day 90	As(V)	0.196	0.03	0.07	1.17	5.19	0.96
	Se(VI)		0.00	0.32	1.41	13.74	0.87
	Fe		1.00	0.22	0.98	0.94	0.99
	Sr		0.95	0.28	1.61	1.10	0.99

[a] hydrodynamic dispersion coefficient;
[b] fraction of sorption sites in contact with mobile water;
[c] immobile water content;
[d] first-order mass transfer coefficient for solute exchange between mobile and immobile water regions;
[e] distribution coefficient.
Using HYDRUS-1D version 4.16 (Šimůnek et al., 2013)

Table 4. Parameter values of physical nonequilibrium simulations of lithium transport in BY soil.

Stage [a]	D (cm^2 min^{-1}) [b]	f_{mo} [c]	θ_{im} [d]	α_s (min^{-1}) [e]	R [f]	R^2
i	0.22	0.99	0.32	0.03	7.72	0.94
ii		0.50	0.17	0.04	5.45	0.93
iii		0.74	0.20	0.24	8.09	0.92

[a] Stage: (i) upon preconditioning with background solution; (ii) at the end of leaching of Day 1 produced water; (iii) at the end of desorption by background solution;
[b] hydrodynamic dispersion coefficient;
[c] fraction of sorption sites in contact with mobile water;
[d] immobile water content;
[e] first-order mass transfer coefficient for solute exchange between mobile and immobile water regions;
[f] retardation factor calculated by using the normalized first temporal moment.
Using HYDRUS-1D version 4.16 (Šimůnek et al., 2013)

Highlights

- Earlier breakthrough of metals with increasing ionic strength of flowback solutions
- Two-region physical non-equilibrium model provided a good fit of metal transport
- Less non-equilibrium transport in Day 14 and Day 90 than Day 1 flowback solutions
- Tracer tests indicated reversible change of transport channels due to leaching
- Sorption/desorption of As(V) and Se(VI) was both pH- and ionic strength-dependent

Insights into the Subsurface Transport of As(V) and Se(VI) in Produced Water from Hydraulic Fracturing Using Soil Samples from Qingshankou Formation, Songliao Basin, China

Season S. Chen[1], Yuqing Sun[1,2], Daniel C.W. Tsang[1,*], Nigel J.D. Graham[2], Yujie Feng[3,*], Yong Sik Ok[4], Xiang-dong Li[1]

Supplementary Information

Equilibrium transport model

$$\theta\frac{\partial C}{\partial t} = \theta D\frac{\partial^2 C}{\partial x^2} - \theta v\frac{\partial C}{\partial x} - \rho\frac{\partial S}{\partial t}$$

where x is distance (cm), t is time (min), ρ is bulk density (g cm^{-3}), θ is water content (dimensionless), D is the hydrodynamic dispersion coefficient (cm^2 min^{-1}), v is average pore-water velocity (cm min^{-1}), C is solution concentration (mol cm^{-3}), and S is sorbed concentration (mol g^{-1}).

The initial condition is:

$C(x,0) = 0$

The boundary conditions are:

$C_0(t) = C_0 \quad 0 < t \leq t_0$

$C_0(t) = 0 \quad t > t_0$

where C_0 is the given concentration of the solute.

Two-region physical nonequilibrium transport model

$\theta = \theta_{mo} + \theta_{im}$

while θ_{mo} is mobile water region (dimensionless) and θ_{im} is immobile water region (dimensionless).

Total concentration in soil (C_T) is:

$C_T = \theta_{mo}C_{mo} + f\rho_b S_{mo} + \theta_{im}C_{im} + (1\text{-}f)\rho_b S_{im}$

where C_{mo} and C_{im} are for mobile and immobile liquid concentrations, and S_{mo} and S_{im} for mobile and immobile adsorbed concentrations, f is the dimensionless fraction of adsorption sites in the mobile region.

Mobile-phase ADE is:

$$\frac{\partial}{\partial t}(\theta_{mo}C_{mo}) + \frac{\partial}{\partial t}(f\rho_b K_d C_{mo}) = \frac{\partial}{\partial z}\left(\theta_{mo}D_{mo}\frac{\partial C_{mo}}{\partial z}\right) - \frac{\partial(J_w C_{mo})}{\partial z} - \Gamma_s$$

Exchange with the immobile phases:

$$\Gamma_s = \alpha_s(C_{mo} - C_{im}) = \frac{\partial}{\partial t}(\theta_{im}C_{im}) + \frac{\partial}{\partial t}[(1-f)\rho_b K_d C_{im}]$$

where α_s is the first-order exchange rate coefficient (min^{-1}) and J_w is the water flux ($cm\ min^{-1}$).

Table S1. Background mobility of As(V) and Se(VI) tested by European Council Waste Acceptance Criteria

	AD	**BY**	**BX**	**DQ**
As(V) ($\mu g\ kg^{-1}$)	27.4	20.7	44.6	35.5
Se(VI) ($\mu g\ kg^{-1}$)	2.26	3.10	31.6	48.1

Table S2. Parameter values of the two-region physical nonequilibrium transport simulations in AD, BX, and DQ soils.

Soil	Solution	Metal	D (cm^2 min^{-1}) [a]	f_{mo} [b]	θ_{im} [c]	α_s (min^{-1}) [d]	K_d (cm^3 g^{-1}) [e]	R^2
AD	Day 1	As	6.075E-4	0.32	0.09	3.40	2.02	0.97
		Se		0.56	0.32	1.62	7.46	0.91
		Fe		0.27	0.02	1.39	1.67	0.96
		Sr		0.20	0.10	1.00	1.48	0.86
	Day 14	As	6.52E-4	0.04	0.08	7.82	1.24	0.95
		Se		0.00	0.25	3.22	2.50	0.96
		Fe		0.03	0.05	1.25	0.74	0.95
		Sr		0.02	0.08	1.31	0.62	0.94
	Day 90	As	5.779E-4	0.21	0.00	4.47	1.00	0.98
		Se		0.56	0.00	2.42	2.37	0.97
		Fe		0.90	0.29	4.13	1.23	0.99
		Sr		0.88	0.29	5.80	1.26	1.00
BX	Day 1	As	0.096	0.13	0.38	5.11	2.50	0.96
		Se		0.11	0.27	5.83	10.18	0.74
		Fe		0.62	0.38	8.30	1.78	0.99
		Sr		1.00	0.12	3.79	1.82	0.96
	Day 14	As	0.093	0.07	0.37	5.57	1.25	0.96
		Se		0.02	0.19	1.89	4.35	0.95
		Fe		0.46	0.38	7.58	1.28	0.98
		Sr		0.14	0.11	11.81	1.35	0.99
	Day 90	As	0.091	0.04	0.38	1.39	4.38	0.94
		Se		0.08	0.38	1.89	19.94	0.87
		Fe		0.56	0.07	4.46	1.19	0.98
		Sr		1.00	0.06	2.48	1.05	1.00
DQ	Day 1	As	1.31E-3	0.49	0.29	3.16	1.77	0.97
		Se		0.35	0.01	7.04	5.92	0.90
		Fe		0.20	0.10	1.00	1.00	0.94
		Sr		0.06	0.38	77.41	1.38	0.92
	Day 14	As	1.30E-3	0.45	0.01	1.50	2.39	0.97
		Se		0.18	0.16	1.52	7.49	0.90
		Fe		0.16	0.05	10.89	1.39	0.95
		Sr		0.42	0.05	5.02	1.61	0.99
	Day 90	As	1.25E-3	0.36	0.34	1.13	6.40	0.93
		Se		0.01	0.34	1.88	13.34	0.92
		Fe		0.69	0.00	3.56	1.69	0.94
		Sr		0.10	0.00	4.55	0.93	0.91

[a] hydrodynamic dispersion coefficient;
[b] fraction of sorption sites in contact with mobile water;
[c] immobile water content;
[d] first-order mass transfer coefficient for solute exchange between mobile and immobile water regions;
[e] distribution coefficient.
Using HYDRUS-1D version 4.16 (Šimůnek et al., 2013)

Table S3. Parameter values of physical nonequilibrium simulations of lithium transport in AD, BX, and DQ soils.

Soil	Stage [a]	D (cm^2 min^{-1}) [b]	f_{mo} [c]	θ_{im} [d]	K_d (cm^3 g^{-1}) [e]	α_s (min^{-1}) [f]	R [g]	R^2
AD	i	0.0007	0.05	0.32	2.09	0.70	8.55	0.93
	ii		0.01	0.03		0.18	5.08	0.97
	iii		0.12	0.24		0.27	7.39	0.94
BX	i	0.095	0.65	0.00	2.82	1.37	8.67	0.96
	ii		0.03	0.38		0.34	8.29	0.84
	iii		0.27	0.00		0.63	9.20	0.90
DQ	i	0.0012	0.97	0.21	2.24	0.39	7.42	0.92
	ii		0.13	0.27		0.27	5.92	0.87
	iii		0.20	0.20		0.87	6.83	0.94

[a] Stage: (i) upon preconditioning with background solution; (ii) at the end of leaching of Day 1 produced solution; (iii) at the end of desorption by background solution;
[b] hydrodynamic dispersion coefficient;
[c] fraction of sorption sites in contact with mobile water;
[d] immobile water content;
[e] distribution coefficient;
[f] first-order mass transfer coefficient for solute exchange between mobile and immobile water regions;
[g] retardation factor calculated by using the normalized first temporal moment.
Using HYDRUS-1D version 4.16 (Šimůnek et al., 2013)

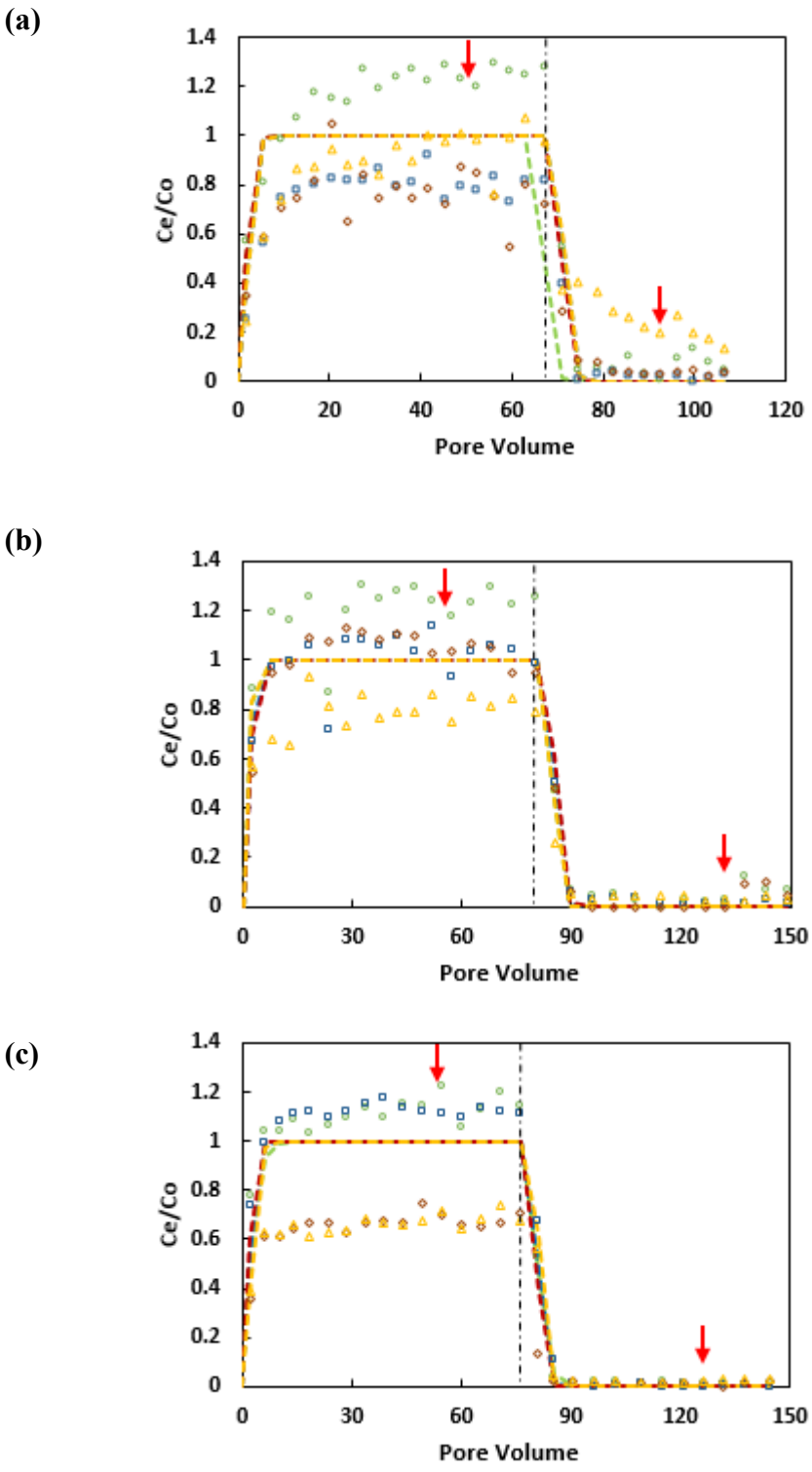

Figure S1. Equilibrium model simulations of metal/metalloid transport in BY soil: (a) Day 1 solution; (b) Day 14 solution; (c) Day 90 solution (experimental data: ◇ As(V), △ Se(VI), □ Sr, ○ Fe; two-region physical nonequilibrium model simulation: —As(V), —Se(VI), —Sr, —Fe; the dashed line indicated end of sorption phase; the arrows indicated flow interruptions during sorption phase and desorption phase, respectively).

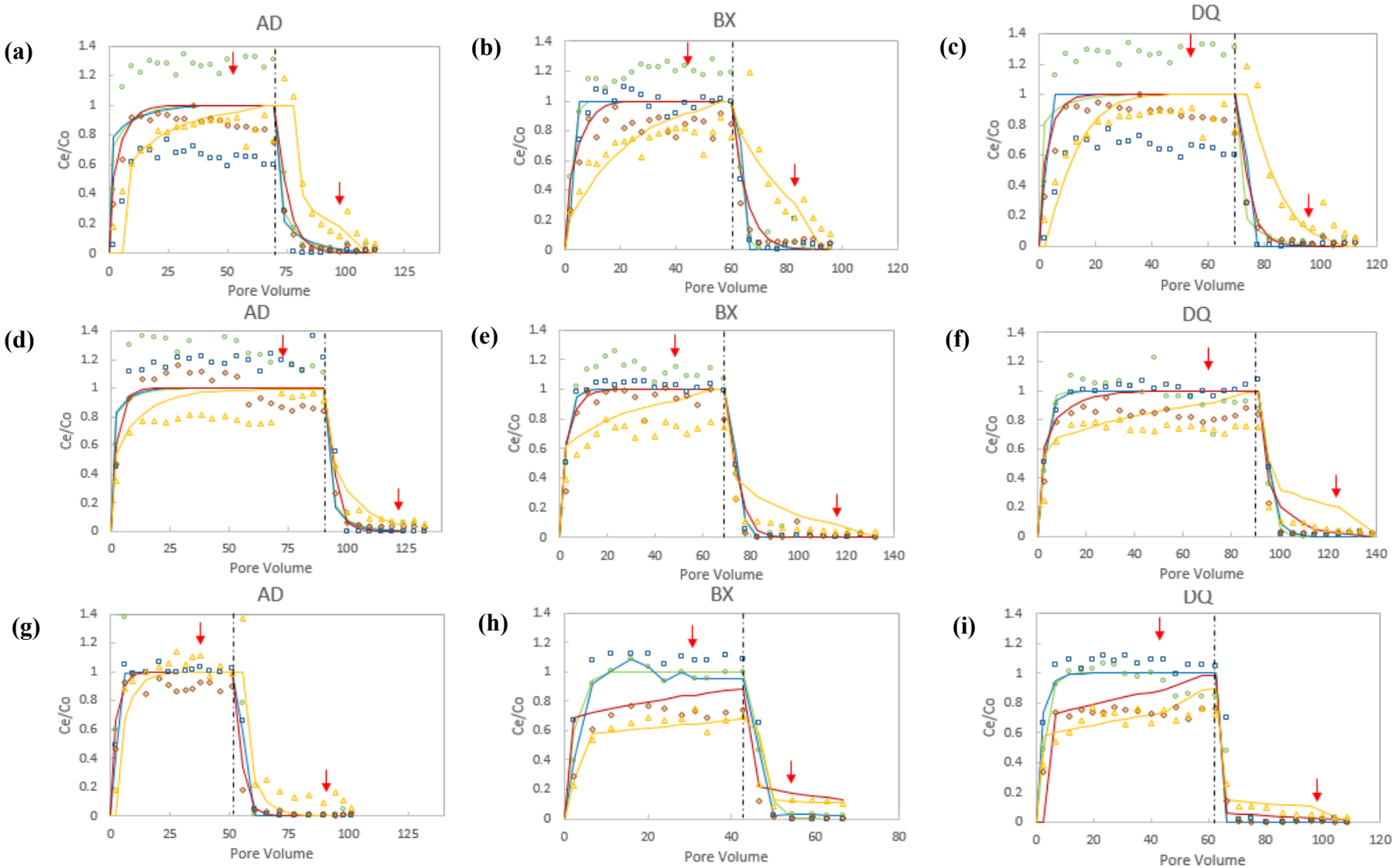

Figure S2. Breakthrough curves of metal/metalloid transport in AD, BX, and DQ soils: (a-c) Day 1 solution; (d-f) Day 14 solution; (g-i) Day 90 solution (experimental data: ◇ As(V), △ Se(VI), □ Sr, ○ Fe; two-region physical nonequilibrium model simulation: —As(V), —Se(VI), —Sr, —Fe; the dashed line indicated end of sorption phase; the arrows indicated flow interruptions during sorption phase and desorption phase, respectively).

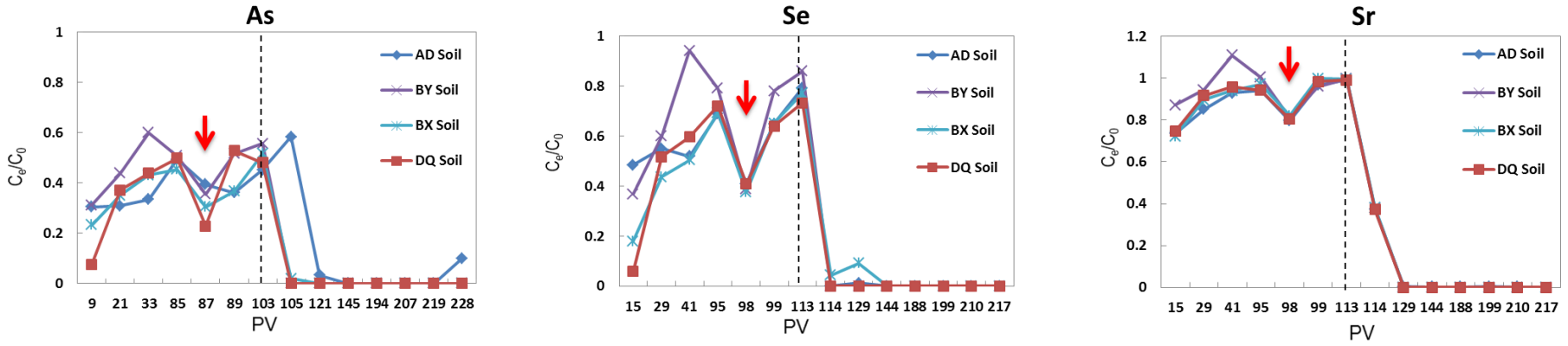

Figure S3. Preliminary results of metal/metalloid transport in columns with a blend of 20% sand by mass (arrow indicated flow cessation, and the dashed line indicated end of sorption phase).

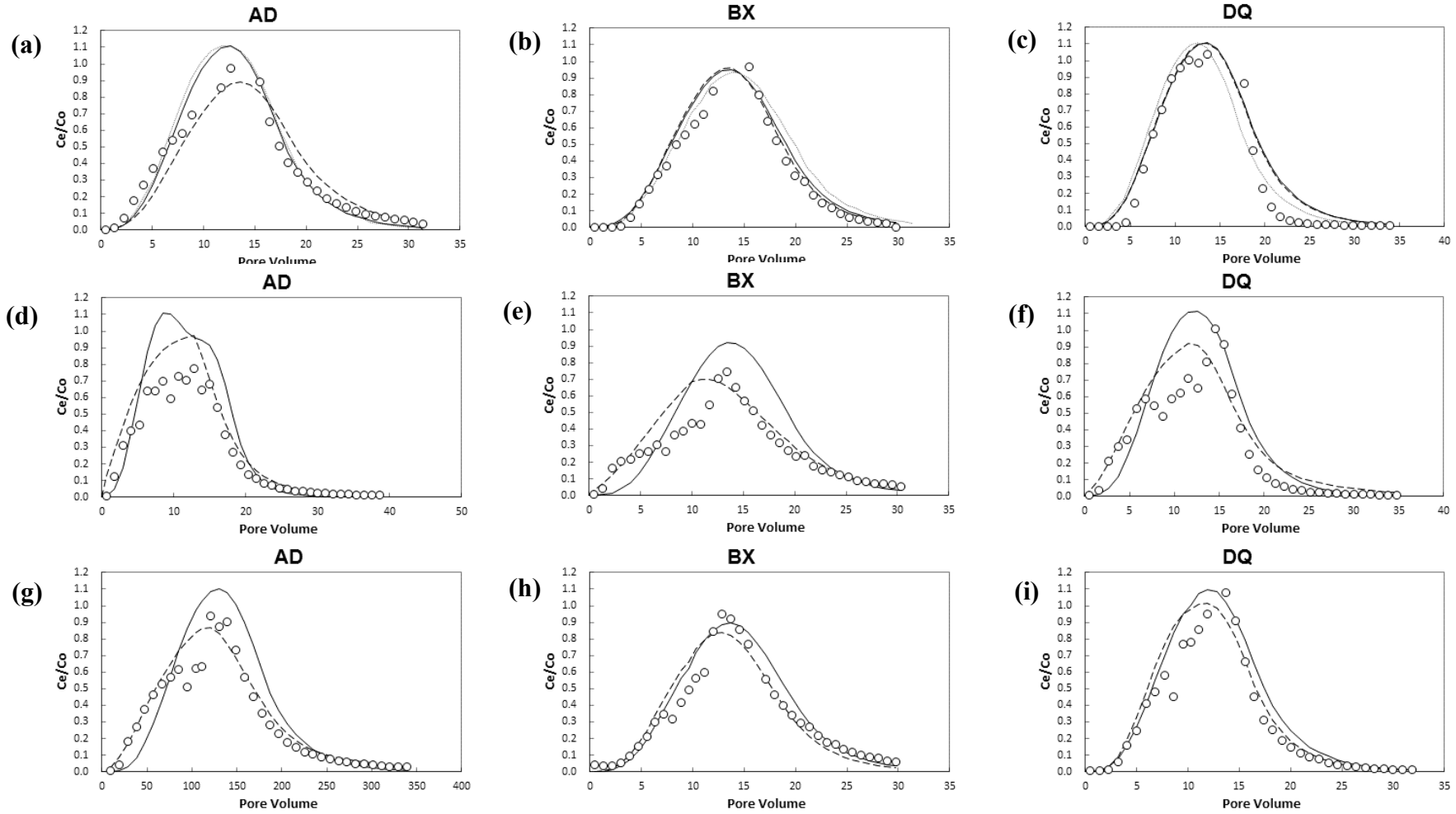

Figure S4. Lithium tracer breakthrough curves in AD, BX, and DQ soils: (a-c) upon preconditioning with background solution; (d-f) at the end of leaching of Day 1 solution; and (g-i) at the end of desorption by background solution (○ experimental data; ——equilibrium model simulation; – – – two-region physical nonequilibrium model simulation; ····· direct simulation).

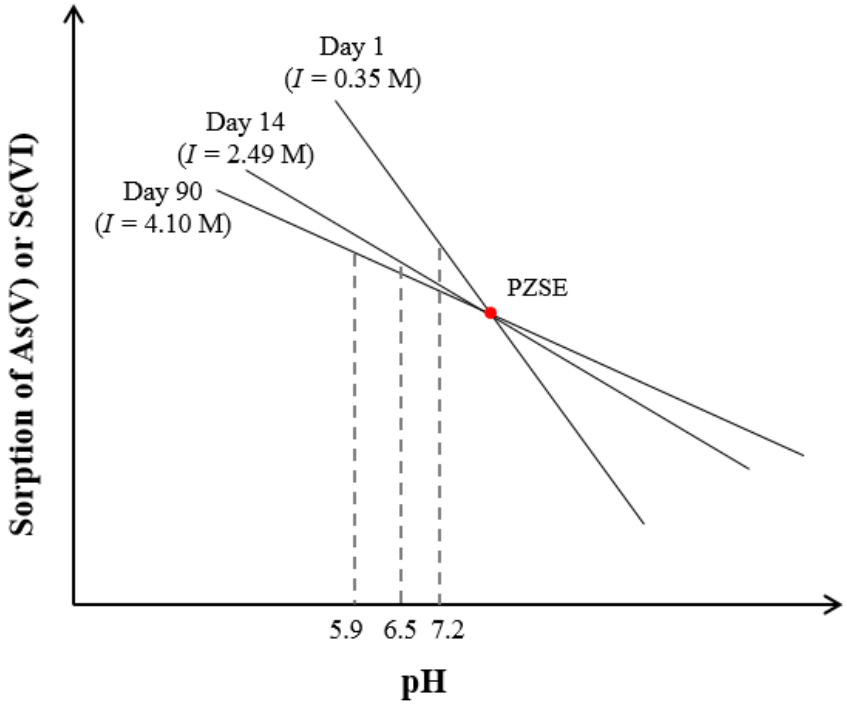

Figure S5. Illustration of pH and ionic strength effects on the sorption of As(V) and Se(VI) on soils (PZSE: point of zero salt effect).

References:

1) Šimůnek, J., Th. Van Genuchten, M. 2008. Modeling nonequilibrium flow and transport processes using HYDRUS. Vadose Zone J. 7, 782-797.
2) Šimůnek, J., Šejna, M., Saito, H., Th. Van Genuchten, M. The HYDRUS-1D software package for simulating the one-dimensional movement of water, heat, heat, and multiple solutes in variably-saturated media. Version 4.17. June 2013. Department of Environmental Sciences, University of California Riverside, US.